FEM Based Statistical Data-Driven Modeling Approach for MFT Design Optimization

M. Mogorovic and D. Dujic

FEM Based Statistical Data-Driven Modeling Approach for MFT Design Optimization

Marko Mogorovic, *Member, IEEE,* Drazen Dujic, *Senior Member, IEEE*

Abstract—This paper proposes a novel class of neural-network inspired statistical data-driven models, especially derived for the purpose of design optimization of medium frequency transformers. These models allow for an efficient ($3 - 5$ orders of magnitude faster compared to FEM), yet sufficiently accurate (within $5 - 10\%$ error relative to FEM) and numerically stable estimation of the complex effects, with otherwise impractically high computational cost and/or convergence issues. The application of the proposed modeling framework is described in detail on two characteristic examples of the complex electromagnetic phenomena occurring within the medium frequency transformers. The performance of the derived models is verified both with detailed FEM simulations and experimental results.

Index Terms—MFT, modeling, design, optimization, power electronics

NOMENCLATURE

H	Magnetic field
W	Magnetic field energy
A	Core limb width
B	Core window area width
C	Core window area height
D	Core depth
MLT	Equivalent mean length turn of the center of weight of the magnetic energy
PW, SW	Primary and secondary winding, respectively
IWA	Minimal rectangular area around the windings
d_{w1}	Winding 1 width
d_{w2}	Winding 2 width
d_{w1c}	Winding 1 to core horizontal clearance distance
d_{w2c}	Winding 2 to core horizontal clearance distance
d_{w1w2}	Winding 1 to winding 2 clearance distance
h_{w1}	Winding 1 height
h_{w2}	Winding 2 height
h_{w1c}	Winding 1 to core vertical clearance distance
h_{w2c}	Winding 2 to core vertical clearance distance
dX	Horizontal offset between the centers of the IWA and the core window area
dh_{w2}	Vertical offset between the centers of the IWA and SW
C_{t2c}	Turn-to-core parasitic capacitance
C_{t2t}	Turn-to-turn parasitic capacitance
D_{t2c}	Turn-to-core distance
D_{t2t}	Turn-to-turn distance
W_t	Turn width
H_t	Turn height
R_t	Turn edge radius
N	Number of winding turns
E	Electric field
V	Electric field potential
V_m	Voltage pulse magnitude
t	Time
$a_{i_1 \dots i_n}$	Multi-variable polynomial coefficients
x_i	Normalized variables
$\mathbf{x}_i$	Vector of normalized variables
$f_i(\mathbf{x})$	Multi-variable polynomial function

I. INTRODUCTION

Any design optimization relies on some form of mathematical description of the relevant underlying physics. The quality of the whole process boils down to the right trade-off between accuracy and execution speed of the utilized models. A qualitative and principal comparison of different available classes of models, in this respect, is given in Figs. 1 and 2. On the one side, finite elements method (FEM) provides a detailed and very precise modeling framework, but its computational cost and numeric convergence issues are often prohibitive when dealing with complex geometries featuring coupled multiphysics. On the other side, analytic models usually have a very low computational cost, but offer acceptable accuracy only for a very narrow set of phenomena that can be well analytically described or approximated, as displayed in Fig. 1a.

Without any better alternative, some of the oldest analytic models [1]–[3], developed well before the computational power was sufficiently evolved to allow the numeric solution of partial differential equations via FEM, are now experiencing a renaissance within design optimization applications. Computationally light analytic models perform extremely well as long as the necessary approximations/assumptions hold within reasonable accuracy limits.

Unfortunately, both electromagnetic and heat transfer equations in 3D have an exact closed-form analytic description only for a very limited class of special problems, featuring either full concentric symmetry or extreme relative ratios of certain dimensions that can be considered infinite and edge effects neglected in the averaging. In order to extend the validity range, any other more complex geometry of interest is interpreted as a reduced and approximated equivalent which fulfills one of the two aforementioned properties. However, depending on the strength of the involved assumptions, the estimation errors introduced as a side-effect of this reduction are often a limiting factor.
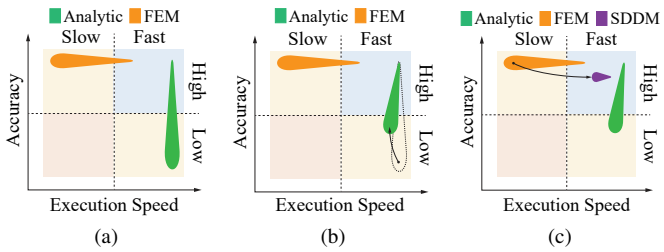
Fig. 1. Qualitative analysis of the properties of various classes of models: (a) Analytic and FEM; (b) Inclusion of various correction factors into analytic models to compensate for simplifications and approximations and improve the estimation accuracy for a number of isolated cases. (c) Inclusion of the proposed FEM-based statistical data-driven models (SDDM) allows modeling complex phenomena with inherent accuracy almost as good as FEM (within $< 5\%$ error) yet with execution speed comparable to analytic models ($3-5$ orders of magnitude faster than FEM).

Fig. 2. Modeling principles: (a) Full numeric modeling, e.g. 3D FEM multiphysics, (b) Full analytic modeling, (c) SDDM modeling.

Therefore, a great deal of scientific effort has been directed into improving many of the aforementioned inherited legacy models - a significant number of corrections (e.g. correction factors) has been developed over the years to compensate for these errors and improve the accuracy of the specific, especially important models, as can be seen in Fig. 1b.

While it is the best when a certain model has an analytic closed form description, there are still problems that cannot be analytically approximated within reasonable accuracy limits. In these cases FEM is normally used. In general, due to high computational cost and problems with numeric stability, these models are usually used for final design verification and its correction through several last iterations outside of the main design optimization loop. This paper proposes a new class of models, FEM based statistical data driven models (SDDM), inherently featuring the high precision of FEM (within $< 5\%$ error compared to FEM) yet with execution speed comparable to analytic models ($3-5$ orders of magnitude faster than FEM), as displayed in Fig. 1c. With this type of modeling framework it is now possible to include very complex and sophisticated simulations, otherwise impractically slow or numerically unstable, into the main optimization loop.

Inspired by neural networks, this methodology uses regression to train the models based on the results of the extensive FEM simulations of the representative generalized geometry details. Models are expressed as multi-variable polynomials, providing a powerful generalized modeling format for a wide spectrum of phenomena with low computational cost.

For the sake of illustration, the approach can be compared to early analytic empirical models, such as Steinmetz equation [2] and many others, with the two key differences: (i) the format of the model is standardized, yet very flexible thus providing a very efficient modeling framework that is applicable to a very wide range of models; (ii) the data gathering cost is very low. In contrast to series of real experiments, relevant data can be obtained through excessive systematically-parametrized FEM simulations and verified with only a few experimental results.

This paper is structured as follows. Two representative application examples of the proposed SDDM modeling framework are provided, on the electromagnetic phenomena that cannot 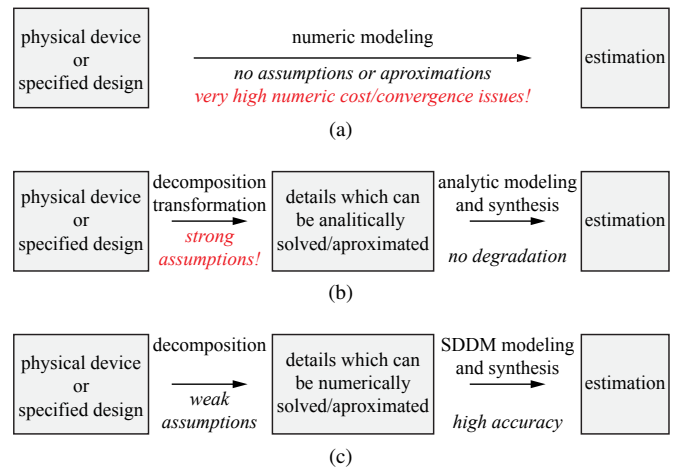be properly analytically modeled. Section II describes the application of the SDDM methodology on the modeling of the leakage inductance of medium frequency transformers (MFTs) with asymmetric winding structures. The identification and normalization of the representative generalized geometry details and the derivation of the multi-variable polynomial models is described in detail. Section III shows how SDDM can be used for modeling of local electrostatic fields for the purposes of insulation coordination of MFTs. Both resulting models are verified with detailed FEM simulations and experimentally on a multi-winding MFT prototype, as provided within the corresponding sections. Section IV provides general conclusions and an outlook based on the presented results.

II. SDDM Leakage Inductance Modeling Of Asymmetric Winding Structures

In solid state transformer (SST) [4] applications, a proper design of the MFT electric parameters, especially the MFT leakage inductance, is important for the proper converter operation [5]. While it is possible to quite accurately model the leakage inductance of the typical symmetric 2-winding transformer geometries, using light-weight analytic models [6]–[8], in case of frequently encountered asymmetric multi-winding structures [9], [10], such as shown in Fig. 3, all of the available methods (e.g. FEM, Roth [11] etc.) resort to some type of computationally intensive numeric techniques. These methods offer excellent accuracy, but their execution time and numeric stability are often limiting factors when it comes to overall multi-variable optimization. To that end, this paper proposes the SDDM as a methodology to generate a computationally efficient DC leakage inductance model for multi-winding transformers with acceptable accuracy.

SDDM is based on multi-variable polynomial fitting of the results of the FEM analysis of the two representative generalized winding geometry primitives, as given in Fig. 4. Thus the proposed model keeps the inherent precision of the FEM as the most precise modeling approach, whereas its execution comes down to several low order matrix multiplications, as one of the most primitive computation functions, resulting in very fast execution.
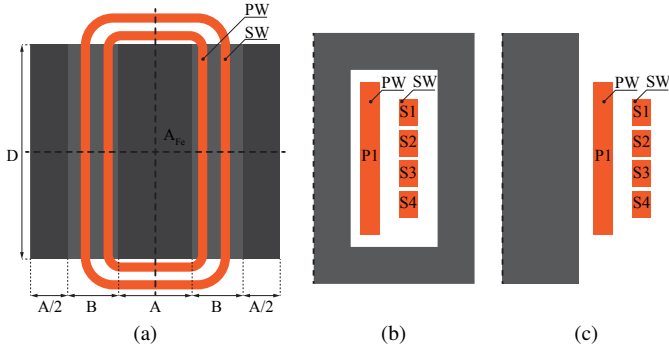
Fig. 3. Considered multi-winding transformer with asymmetric winding structure. (a) Horizontal cross-section showing two axis of MFT geometric symmetry. MFT geometric symmetry detail inside (b) and outside (c) of the core window area.

A. Proposed Modeling Method

While full 3D coupled multiphysics FEM modeling is usually out of the question for optimization of systems with higher complexity, the decoupled simulation of various details is still quite computationally efficient and numerically robust, especially in case of the 2D models. Therefore, the first step of SDDM modeling is the electromagnetic FEM analysis that allows the identification of the effects of various geometric parameters on the transformer DC leakage inductance and the analytic decomposition of the model. As shown in [12], the total (3D) leakage inductance of the transformer can be very well estimated using two 2D models, representing the magnetic field energy inside and outside of the core widow area, as depicted in Fig. 3. Therefore, the estimation of the total (3D) leakage boils down to accurate estimation of the magnetic energy in these two 2D geometries.

The two representative 2D generalized geometry primitives are defined and parametrised, as described in Fig. 4, and normalized, as shown in Tables I and II. As can be seen, they are fully defined with eight and seven normalized parameters, respectively. Due to the largely linear effect on the leakage inductance, relative winding widths can be considered as constant. Based on the preservation of the total magnetic energy (S_W), a winding geometry equivalence with infinitely thin windings can be derived, as given in Fig. 5. The effect of the winding (d_{w1} and d_{w2}) and inter-winding (d_{w1w2}) widths on the leakage inductance can be merged into an equivalent inter-winding distance (1).

$$d_{w1w2.eq} = d_{w1w2} + \frac{1}{3}(d_{w1} + d_{w2}) \tag{1}$$

Using this equivalence, any winding width configuration can be transformed into any other, while preserving the total magnetic energy and consequently the resulting leakage inductance. Of course, in case of the discussed asymmetric winding arrangement, this equivalence is an approximation. However, this is a very good approximation that yields a very accurate result within a large range of different winding widths - covering most of the practical designs.

This is one of the main advantages of SDDM compared to analytic modeling - the decomposition of the initial problem to several simple details is done with no or very little loss of accuracy, as illustrated in Fig. 2. Unlike the analytic models which can be applied only to a very limited class of geometry details with special features, almost any geometry can be solved with FEM. Thus the strong assumptions and approximations (which can significantly affect the modeling accuracy) that are necessary to transform the given geometry up to the point when it can analytically be solved are relaxed. However, it is still important to non-destructively decompose the model to the simplest possible representative details, as applying the SDDM to the full 3D FEM model would again yield all of the original problems with computation cost and numeric stability.

A 2D magnetostatic FEM parametric sweep has been performed, generating the set of leakage inductance estimations (approximately 50'000 simulations) within the geometry range of interest according to Tables I and II, covering all of the practically relevant geometry ratios, as displayed in Figs. 6a and 6b.

Based on these results, and taking into account the minimum vector of influential variables (**x**), as summarized in Tables I and II, a multi-variable polynomial fitting is done variable by variable, as shown in Fig. 7, allowing to always choose the minimum adequate polynomial order while inherently
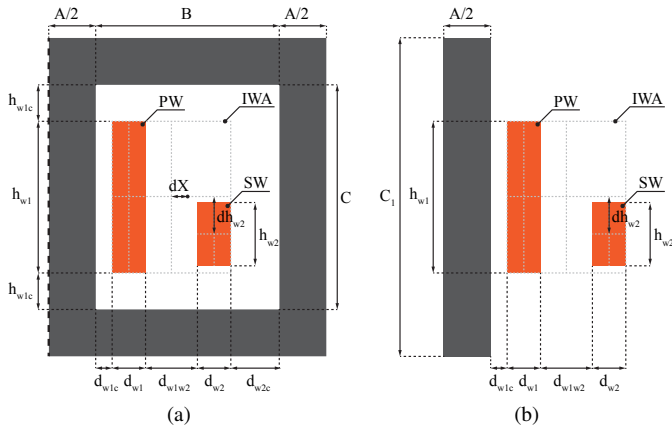

Fig. 4. Two generalized geometry details describing the magnetic energy of the winding cross-section inside (a) and outside (b) of the core window area.
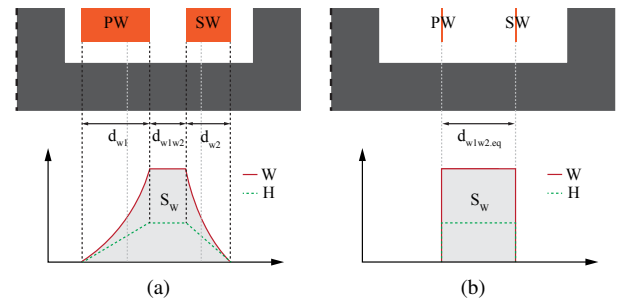

Fig. 5. Winding geometry equivalence in respect to total magnetic energy (S_W) preservation: (a) Standard 2-winding example (b) Theoretical equivalence with infinitely thin windings.

TABLE I: Definition of the normalized variables based on the generalized winding geometry detail, as shown in Fig. 4a

Norm. Vars.	/	/	x_1	x_2	x_3	x_4	x_5	x_6
Definition	$\frac{d_{w1}}{h_{w1}}$	$\frac{d_{w2}}{h_{w1}}$	$\frac{d_{w1w2}}{h_{w1}}$	$\frac{h_{w2}}{h_{w1}}$	$\frac{2dh_{w2}}{h_{w1}-h_{w2}}$	$\frac{B}{d_{w1}+d_{w1w2}+d_{w2}}$	$\frac{C}{h_{w1}}$	$\frac{2dX}{B-d_{w1}-d_{w1w2}-d_{w2}}$
Range	0.1	0.1	[0, 0.7]	[0.2, 1]	[0, 1]	[1, 2]	[1, 2]	[−1, 1]

Note that h_{w1} is taken as a reference when defining the geometry ratios. Winding widths (d_{w1} and d_{w2}) are fixed as their effect on the leakage is quite linear and can be taken into account through a correction of d_{w1w2}.

TABLE II: Definition of the normalized variables based on the generalized winding geometry detail, as shown in Fig. 4b

Norm. Vars.	/	/	x_1	x_2	x_3	x_4	x_5
Definition	$\frac{d_{w1}}{h_{w1}}$	$\frac{d_{w2}}{h_{w1}}$	$\frac{d_{w1w2}}{h_{w1}}$	$\frac{h_{w2}}{h_{w1}}$	$\frac{2dh_{w2}}{h_{w1}-h_{w2}}$	$\frac{d_{w1c}}{d_{w1}+d_{w1w2}+d_{w2}}$	$\frac{C}{h_{w1}}$
Range	0.1	0.1	[0, 0.7]	[0.2, 1]	[0, 1]	[0, 1]	[1, 2]

Note that compared to the geometry detail inside the core window area (Fig. 4a), the leakage inductance is in this case fully defined by five normalized variables. Instead of x_4 and x_6 from Table I, it is enough to define x_4 as given in Table II.
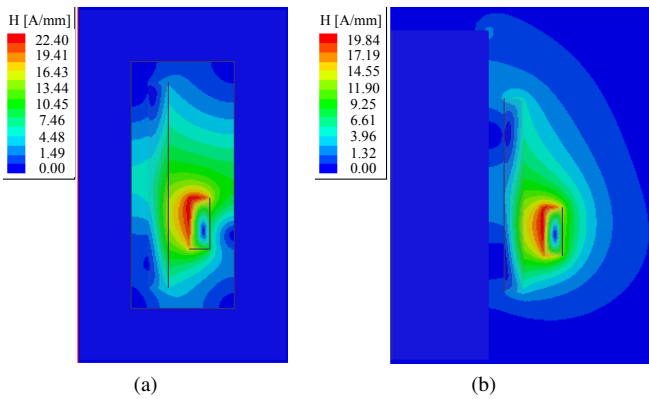

Fig. 6. An example of the 2D magnetostatic FEM simulation of the magnetic field inside (a) and outside (b) of the core window area.

Fig. 7. Multi-variable polynomial fitting of the MFT leakage inductance to the results of the 2D FEM sweep (approximately 50'000 simulations).

ensuring convergence. This is done using a custom made algorithm that employs the polyfit function from the numpy python library for single-variable polynomial fitting, based on minimum square error method. Several transformations of the normalized variables, employing typical fitting functions, such as e^x, $\log(x)$ and $1/x$ are used to linearize the data sets as much as possible in order to achieve a better fit. The final result of this fitting is a multi-dimensional array of polynomial parameters. For the sake of illustration, an example of the described model, for a two variable case is shown in (2).

$$L'_{\sigma.fit} = \begin{bmatrix} x_1 \\ 1 \end{bmatrix}^T \begin{bmatrix} a_{1.3} & a_{1.2} & a_{1.1} & a_{1.0} \\ a_{0.3} & a_{0.2} & a_{0.1} & a_{0.0} \end{bmatrix} \begin{bmatrix} x_2^3 \\ x_2^2 \\ x_2 \\ 1 \end{bmatrix} \quad (2)$$

As can be seen, the evaluation of the model boils down to a simple low-order matrix multiplication. While this operation executes very fast on the processor, depending on how many variables (N) are involved, and what are the orders of the polynomial fittings (n_i), there is $\prod_{i=1}^{N} n_i$ polynomials to be solved. Although this model is still executing very fast for the case of 6-variables, described by Fig. 4 and Tables I and II
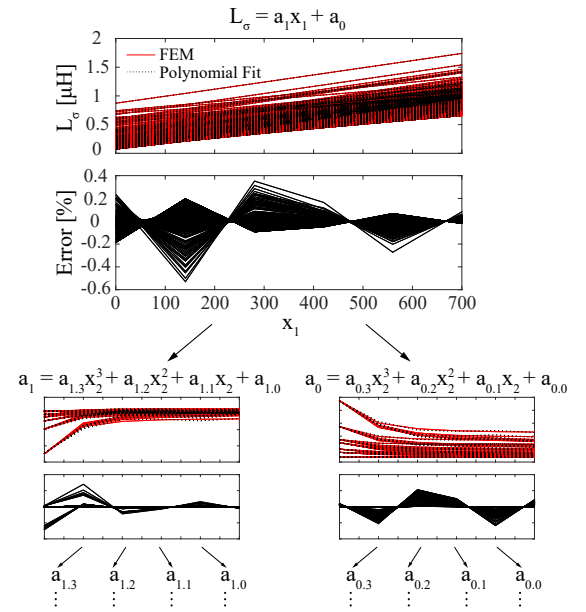
(three orders of magnitude faster compared to FEM), it is possible to further optimize the model. Rearranging the order in which the polynomial is executed based on the algorithm allows for a part of the multi-variable polynomial, involving variables that have been defined, to be pre-calculated and only execute the part of the model dealing with optimization variables within the optimization loop. Doing this, in case that not all of the variables ($\mathbf{x}$) are being actively changed in the most nested optimization loop, it is possible to even further improve the overall execution time.

The resulting multi-variable polynomial models of the two geometric primitives from Fig. 4 have been compared to the results of the FEM sweep, as displayed in Fig. 8. As can be seen, the errors are very low (below 4% for any practical design), confirming the good precision of the model.

While the estimation time is a parameter which strongly depends on the computer hardware and allocated computation
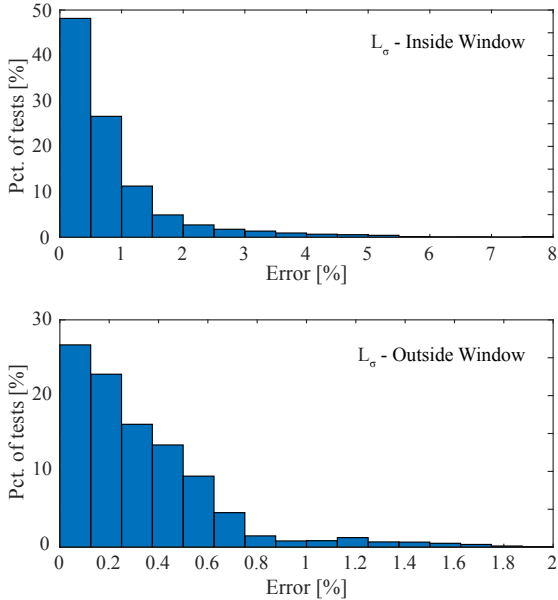
Fig. 8. Histograms of the relative leakage inductance estimation error, referred to the FEM results (approximately 50'000 test samples).

TABLE III: Computation times Fig. 14c

Model	3D FEM	2D FEM	SDDM	Analytic
Ex. [sec]	11.6	2.16	$5.6 \cdot 10^{-4}$	$7.2 \cdot 10^{-5}$

Except for 3D FEM, each execution time is derived as the average time of 50'000 executions, in order to remove any pre-processing/compile time. To get a fair comparison, each application was run as a single-thread. Note that analytic (Dowell's) model is just used for the sake of execution time comparison - as aforementioned analytic models are not suitable for this type of highly asymmetric geometries.

resources, just for the sake of illustration, the execution times of the 3D FEM, 2D FEM, SDDM and analytic Dowell's [3] model are provided in Table III, confirming the aforementioned execution time scale. Note that analytic (Dowell's) model is just used for the sake of execution time comparison.

B. Application of the Model

The application of the derived model is demonstrated on a nine-secondary multi-winding transformer prototype, as displayed in Fig. 10, with a geometry profile, as shown in Fig. 3. Calculation of the total 3D leakage inductance boils down to a few simple steps. First, the dimensions of the two geometric profiles of the MFT, as seen in Fig. 4, need to be identified and transformed using (1) according to Tables I and II. This leads to

$$d_{w1w2.eq01} = d_{w1w2} + \frac{1}{3}\left(d_{w1} + d_{w2} - \frac{2}{3}0.1h_{w1}\right) \quad (3)$$

where $d_{w1w2.eq01}$ is the equivalent inter-winding dielectric distance of the generalized geometry primitive with selected constant normalized winding widths ($0.1h_w$).

Taking into account (3), the two multi-variable polynomial models (f_1 and f_2), describing the magnetic energy inside and outside of the core window area are evaluated leading to per-length permeances, i.e. leakage inductances per-square-turn

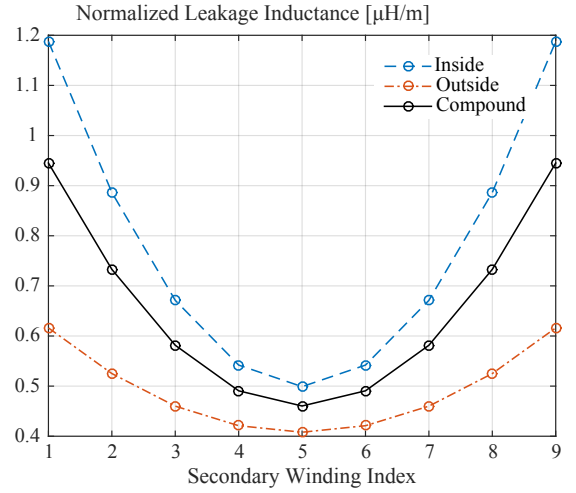$$L'_{\sigma.in} = f_1(\mathbf{x}_1) \quad (4)$$

Fig. 9. An example of the per-length per-square-turn primary to i-th secondary winding leakage inductance calculation of a multi-winding transformer with a geometry profile, as shown in Fig. 3, in case of nine secondary windings, according to the prototype, as given in Fig. 10.
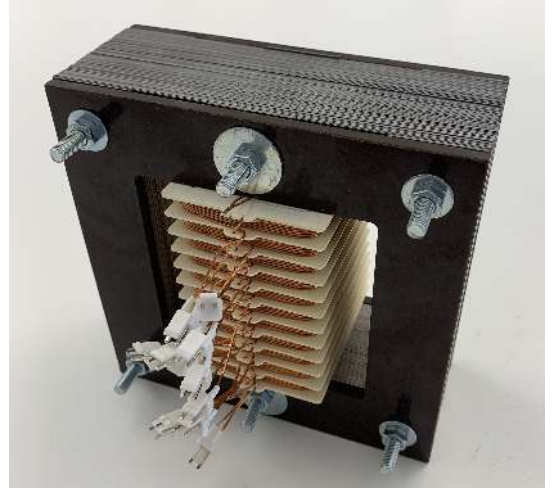

Fig. 10. A multi-winding transformer prototype for experimental verification [13].

$$L'_{\sigma.out} = f_2(\mathbf{x}_2) \quad (5)$$

where $\mathbf{x}_1$ and $\mathbf{x}_2$ are the normalized variable vectors from Tables I and II, respectively. Weighted sum of these two values in respect to the portions of the MLT inside and outside of the core window area (see Fig. 3a) leads to the equivalent per-length permeance, i.e. leakage inductance per-square-turn

$$L'_{\sigma.eq} = \frac{1}{A+D}(DL'_{\sigma.in} + AL'_{\sigma.out}). \quad (6)$$

For the sake of illustration, plots of these values are provided in Fig. 9, for the given transformer prototype. Finally, the total leakage inductance referred to the primary winding of the transformer can be calculated, as shown in (7).

$$L_{\sigma.total} = N_1^2 (MLT) L'_{\sigma.eq} \quad (7)$$

Depending on the design task, beside the direct estimation, this fast executing model also facilitates simple and numerically efficient inverse calculation of any single or arbitrary
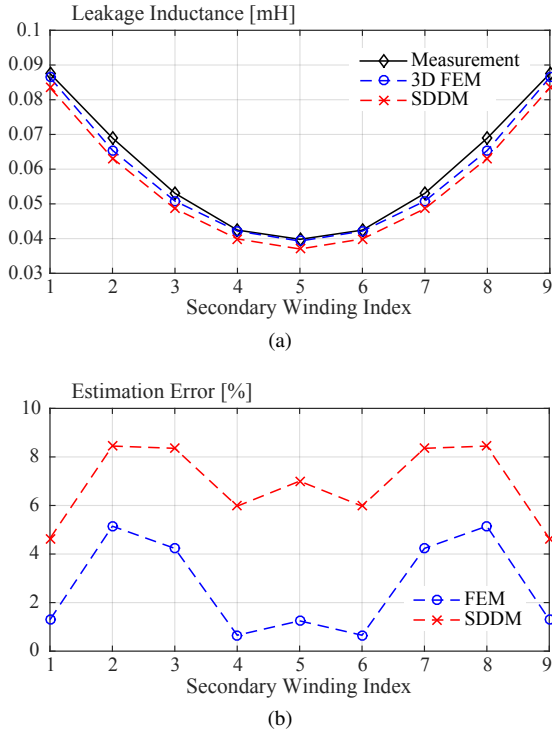
(a)

(b)

Fig. 11. (a) Plots of the measured and estimated (both with the 3D FEM and the proposed SDDM) total primary to i-th secondary winding leakage inductance of the multi-winding transformer prototype from Fig. 10 referred to each secondary winding. (b) Plots of the relative estimation errors of the 3D FEM and the proposed SDDM referred to the measurements.

combination of geometric dimensions **x** (e.g. d_{w1}, d_{w1}, d_{w1w2}) in order to match the reference leakage inductance.

C. Experimental Verification

The presented modeling is verified with a full 3D FEM model and measurement on a muti-winding transformer prototype [13], as displayed in Fig. 10, with geometry profile, as shown in Fig. 3, with nine secondary windings. All of the geometric dimensions, construction details and leakage inductance measurement between each secondary and primary winding can be found in [13].

Plots of the measured and estimated total leakage inductance between the primary and each of the secondary windings and relative estimation errors are displayed in Fig. 11. Estimation is done both with proposed statistical data-driven model (SDDM) and full 3D FEM for comparison purposes. A slight under estimation of the total leakage can be observed for both models. This is most likely due to a small additional leakage inductance of the extended termination of the windings and connection cables. As expected the proposed SDDM performs within the 5% error compared to FEM, achieving good accuracy with less than 9% error compared to the measurement even in case of such extreme geometry ratios.

III. MODELING OF THE LOCAL ELECTRIC FIELD WITHIN THE MFT INSULATION

Similar to the previous, this section proposes the SDDM as a methodology to derive a sufficiently-accurate (error $< 5\%$
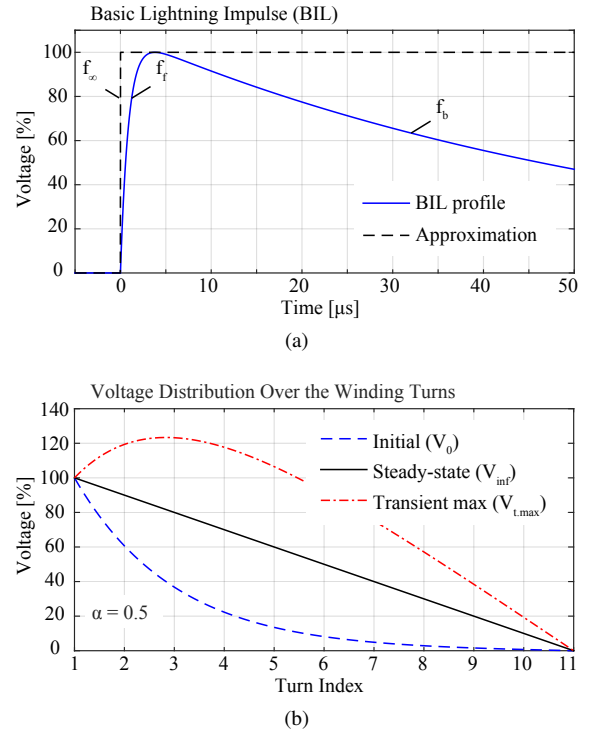

(a)

(b)

Fig. 12. (a) Standard $1.2/50\,\mu s$ full-wave lightning impulse profile, according to IEEE Std 4-1995 and IEEE Std C57.98-1993 (equivalent frequencies of the fast rising front and slow descending back are $f_f = 200$ kHz and $f_b = 5$ kHz, respectively). (b) Example of the theoretical envelope of the voltage distribution over the transformer winding turns during fast "ringing" transients where: V_0 is the initial voltage distribution at $t = 0$; V_{tm} is the maximum theoretical turn voltages during subsequent "ringing" transient; V_{inf} is the voltage distribution after the fast transient response has transpired.
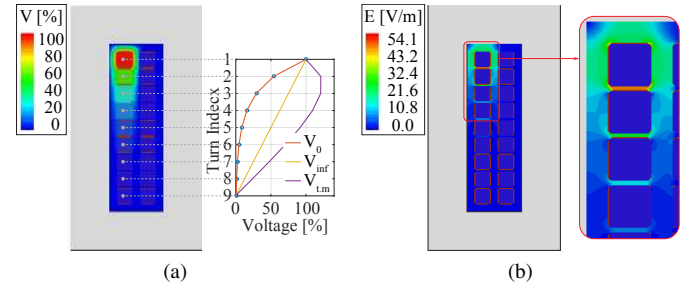

Fig. 13. 2D electrostatic FEM simulation of a representative MFT cross-section example, excited with a theoretical BIL approximation (Heaviside step function) at the moment of incidence ($t = 0$): (a) voltage distribution and (b) E-field distribution.

referred to 2D FEM) models for parasitic capacitance and local E-field maximum estimation within the MFT dielectric material, specially designed for very fast execution - more than four orders of magnitude faster compared to 2D FEM.

Insulation coordination is an essential step in the design process of any medium (MV) or high (HV) voltage power transformer that ensures its proper and safe operation. This task is especially challenging in case of medium (MF) and high (HF) frequency transformers operating within power electronics converters - increasingly popular SST concept [14]. Whether it is a fast rising front of the basic lightning impulse (BIL) test waveform, as shown in Fig. 12a, or very

fast switching of the new generation SiC semiconductors, parasitic capacitances of the transformer windings will affect the voltage and electric (E)-field distribution over the winding turns during these fast transients, as displayed in Figs. 12b and 13, and therefore cannot be neglected [15], [16].

However, due to high complexity, computational cost and need for customization of FEM models, very precise models such as described in [15], [16] are not suitable for overall multi-variable design optimization, but rather for final design verification and its correction through several iterations [5], [14], [17], [18]. In contrast to this, the computationally-efficient and numerically-stable SDDM models, that are derived in this section allow for a proper inclusion of the insulation coordination considerations within the design optimization process.

For the purposes of design optimization, the BIL is approximated with a Heaviside step function as a worst case scenario, as displayed in Fig. 12a. This approximation allows the reduction of the complex HF winding model, to a network of parasitic capacitances, as shown in Fig. 14a, which can be analytically solved in closed form, as given in

$$V(i) = V \frac{\sinh(\alpha i)}{\sinh(\alpha N)} \quad \text{where} \quad \alpha = \sqrt{\frac{C_{t2c}}{C_{t2t}}} \quad (8)$$

where i is the winding turn index, N is the total number of turns and C_{t2c} and C_{t2t} are the turn-to-core and turn-to-turn parasitic capacitances, respectively.

The voltage and E-field distribution over the transformer winding excited with Heaviside step function, at the moment of the pulse incidence ($t = 0$), are shown in Figs. 13a and 13b, respectively. It can be seen that the initial voltage distribution over the winding turns (V_0) is uneven - the first turns are experiencing turn-to-turn voltages drastically above the nominal value. Moreover, some turns experience high, above-nominal, absolute voltage levels during the fast transient on natural frequency of the winding (V_{tm}). This causes high local E-field magnitude-peaks that may lead to gradual (or in extreme cases instant) annihilation of the insulation material if not properly accounted for.

A good understanding of the main parameters governing this phenomena is necessary for the proper insulation coordination. From a design point of view, reliable modeling is paramount in order to avoid massive and costly over-sizing.

A. Proposed Modeling

A detailed electrostatic finite elements method (FEM) analysis is performed to identify the critical regions, where the insulation material is experiencing the highest dielectric stress. As can be seen in Fig. 13b, the maximum local E-field magnitude peaks are occurring somewhere along the conductor edge. These local E-field maximums are a function of the geometry and voltage distribution. On the other hand, assuming the Heaviside step excitation, the voltage distribution is purely a function of turn-to-core and turn-to-turn parasitic capacitances, which again depend only on the geometry. Therefore, in order to predict the maximum local E field peaks, it is necessary to:

(i) Model the parasitic capacitances, based on the known design geometry

TABLE IV: Definition and range of the normalized parameters, according to Fig. 14c

Norm. Var.	x_1	x_2	x_3	x_4	x_5
Definition	$\frac{H_t}{W_t}$	$\frac{D_{t2t}}{W_t}$	$\frac{D_{t2c}}{H_t}$	$\frac{R_t}{\min(H_t, W_t)}$	$\frac{U_{t2t}}{U_{t2c}}$
Range	[0.25, 4]	[0.01, 4]	[0.01, 4]	[0.02, 0.5]	[0, 1]

Note that these are very extensive ranges, covering most of designs
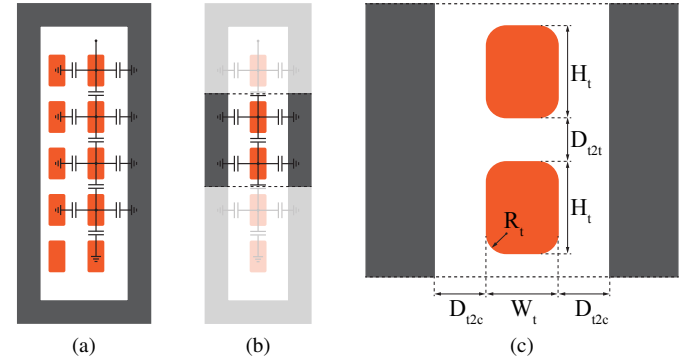

Fig. 14. (a) Full parasitic capacitance model of a generalized MFT geometry cross-section. (b) Simplified geometry equivalence. (c) Minimal generalized geometry detail.
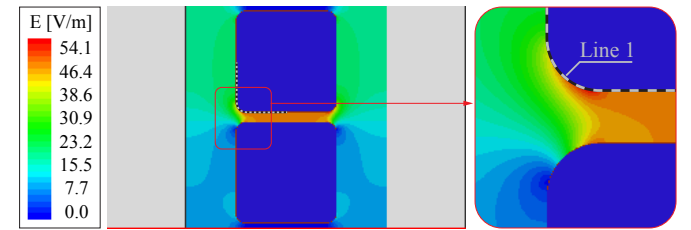

Fig. 15. 2D electrostatic FEM simulation of the minimal generalized geometry detail.

(ii) Solve the parasitic capacitance network to obtain the voltage distribution

(iii) Model the local E-field maximum, based on the known geometry and voltage distribution

While (ii) comes down to a simple evaluation of (8) in case of Heaviside step-function excitation, (i) and (iii) remain numerically challenging.

A full parasitic capacitance network can be seen in Fig. 14a. Taking into account that both the core and secondary winding are at the ground potential, the secondary winding can also be seen as a straight wall boundary at the ground potential, as shown in Fig. 14b. Note that, all conductive parts of the transformer, including any other winding except the one being excited by the test pulse, are grounded at all terminals during the BIL test, as recommended by IEEE Std 4-1995 and IEEE Std C57.98-1993. Finally, based on the geometric symmetry and periodic structure of the winding, a minimal generalized geometry detail, capable of capturing all of the phenomena of interest, is identified and parametrised, as given in Fig. 14c and Table IV.

A 2D FEM parametric sweep is performed on the generalized geometry detail (Fig. 15), as defined in Table IV, extracting the turn-to-core and turn-to-turn parasitic capac-
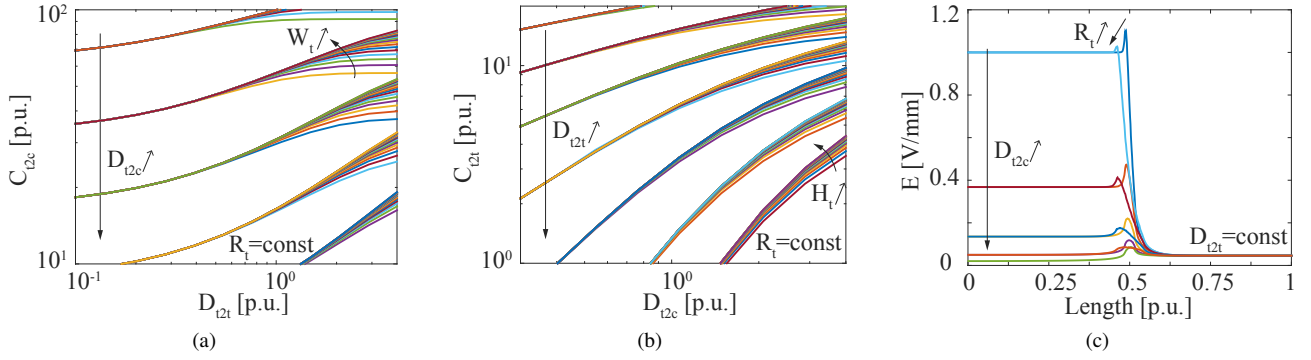
Fig. 16. Plots of families of curves, exposing the effects of various parameters, as given in Table IV, on: (a) turn-to-core $C_{t2c} = f_1(x_1, x_2, x_3, x_4)$, (b) turn-to-turn $C_{t2t} = f_2(x_1, x_2, x_3, x_4)$ parasitic capacitances and (c) the local E-field magnitude peak along the edge of the turn conductor $E_{max} = f_3(x_2, x_3, x_4, x_5)$, as highlighted with Line 1 in Fig. 15.
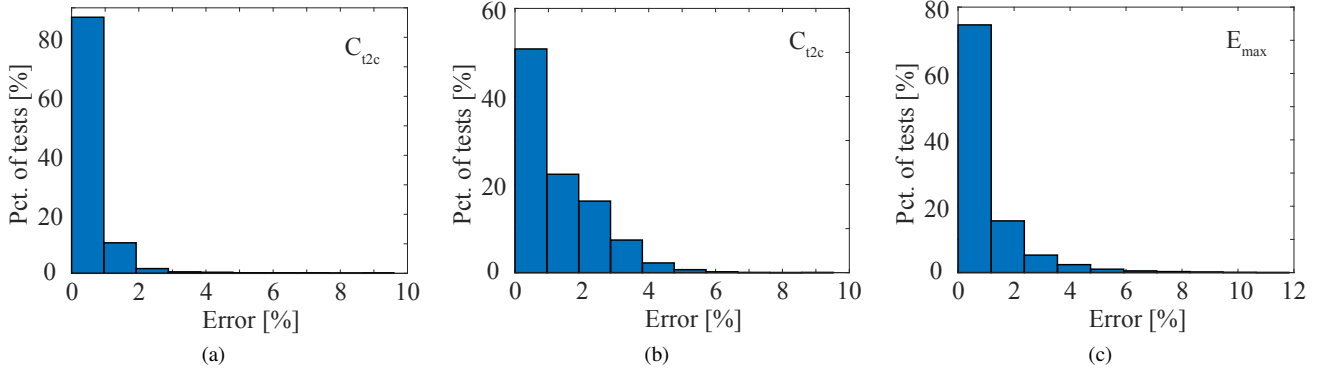

Fig. 17. Relative estimation error histograms (approximately 40'000 simulations) of the proposed data-driven statistical models for computation of: (a) turn-to-core parasitic capacitance, (b) turn-to-turn parasitic capacitance and (c) maximum local E-field magnitude peak.

itances and maximum local E-field peaks at approximately 40'000 points within the parameter ranges of interest. Sample plots of this data, illustrating the effects of various parameters on the modeled values are shown in Fig. 16. Taking into account the minimum vector of influential variables ($\mathbf{x}$), as summarized in Table IV, a multi-variable polynomial fitting is performed on these data sets in the same fashion, as described in Section II, thus generating the corresponding data-driven statistical models

$$C_{t2c} = f_1(x_1, x_2, x_3, x_4) \tag{9}$$

$$C_{t2t} = f_2(x_1, x_2, x_3, x_4) \tag{10}$$

$$E_{max} = f_3(x_2, x_3, x_4, x_5) \tag{11}$$

with inherent high accuracy of FEM simulations and very low computational cost, characteristic for simple arithmetic operations (matrix multiplications) needed for evaluation of polynomials.

As described in Section II, the evaluation of these models boils down to simple low order matrix multiplications which execute very fast on the processor. In case of 4-variables, as described by Fig. 14c, Table IV, and Fig. 16, these models execute more than four orders of magnitude faster than 2D FEM.

All three models ((9), (10) and (11)) are derived under assumption of surrounding vacuum. A different insulation material can easily be taken into account with a simple multiplication/division with its relative permittivity ε_r. Moreover, note that the formula for local E-field maximum is a function of the voltage distribution and therefore covers all relevant voltage distributions that may be encountered during normal (V_{inf}) or transient operation (V_0 and V_{tm}).

B. Simulation Results

Relative estimation errors of the three earlier mentioned multi-variable polynomial models referred to the 2D FEM simulation results are given in Fig. 17. It can be seen that a very good accuracy can be achieved, with errors practically below 5%. Equations (8)-(11) together formulate a framework for a computationally efficient estimation of the local E-field maximums allowing the study of separate influences on insulation coordination and overall design optimization.

While these formulas fully cover the simplest case of single layer windings, discussed in this wok, additional formulas would have to be derived to take into account more complex cross-layer turn-to-turn parasitic couplings of the multi-layer winding structures. Finally, while these models facilitate the inclusion of many insulation coordination considerations into design optimization, they are still a simplified representation of the transformer and a detailed 3D FEM analysis is still advised as a final verification prior to prototyping.
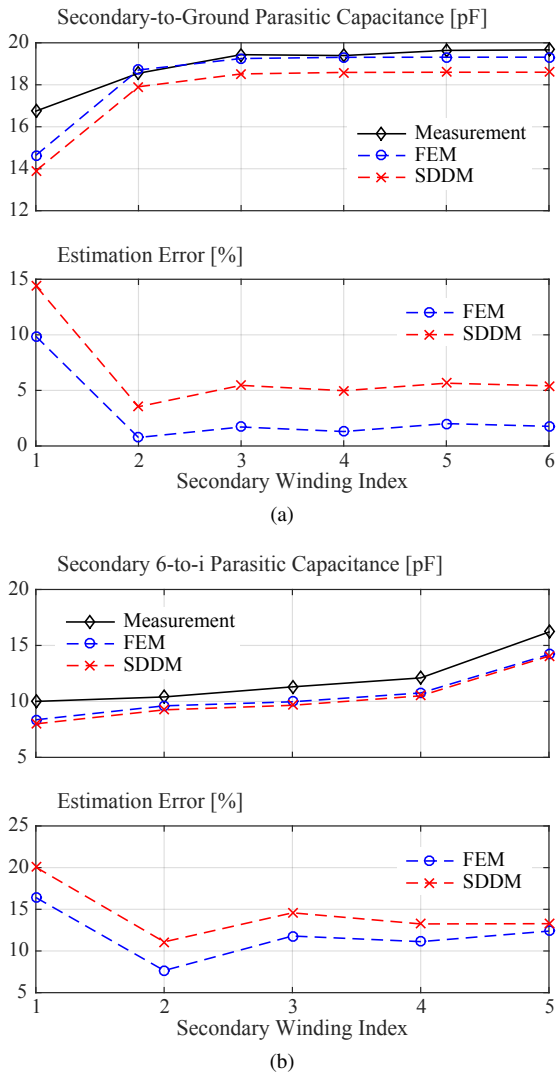
Fig. 18. Relative estimation error histograms of the proposed data-driven statistical models for computation of: (a) turn-to-core parasitic capacitance, (b) turn-to-turn parasitic capacitance and (c) maximum local E-field magnitude peak.

C. Experimental Verification

For the purposes of experimental verification, the same multi-winding transformer prototype has been used, with the winding arrangement, as displayed in Fig. 3 - a single primary and the secondary winding split into 11 partitions. While it is not possible to obtain the measurements of the local electric field peaks, the parasitic capacitance models can be verified on such a prototype.

Unfortunately, the separate parasitic couplings, as described by (9) and (10) cannot be directly measured. Only the total capacitance including all of the couplings can be experimentally obtained between any two elements. Bode 100 vector network analyzer is used to measure the total parasitic capacitance between each secondary and the primary winding, as well as between each secondary and the middle (6th) secondary winding of the multi-winding transformer prototype, as given in Fig. 10.

The estimated value of these total coupling parasitic capacitances can be obtained from the total winding parasitic capacitance network, as shown in Fig. 14a, using the Krone reduction on its admittance matrix. With this operation the total capacitance matrix can be reduced to one equivalent capacitance between any two given nodes. These total parasitic couplings are a function of the separate parasitic couplings described by (9) (turn-to-core and turn-to-primary winding) and (10) (turn-to-turn) and therefore only as accurate as the associated SDDM models.

The plots of the aforementioned total secondary-to-primary and secondary-to-secondary parasitic capacitance measurements and their estimation are shown in Fig. 18. It can be seen that, as expected, the SDDM models are within the 5% error range compared to FEM results. Moreover, the relative error referred to the measurement results is below 20% which is a good result considering the very low value and sensitivity of these parameters.

IV. CONCLUSION

While analytic models can solve a significant set of problems, still many electromagnetic phenomena cannot be accurately described in that way. A computationally efficient, yet sufficiently accurate, statistical data-driven modeling framework based on FEM simulations of simple geometry details and muti-variable polynomial fitting is presented in this paper.

The proposed modeling framework has been described in detail on two representative application examples, showing how it is possible to transform, generalize and normalize a numerically difficult problem up to the point where a sufficiently small set of significant influences (variables) can be very efficiently captured via a neural-network inspired multi-variable polynomial model. Although already very fast (three-four orders of magnitude compared to simple 2D FEM models), these models can also be reorganized for most optimal execution depending on the specific design optimization algorithm and potentially achieve an even more drastic speed improvement. Moreover, a good estimation accuracy is achieved, with errors less than 5% relative to the 3D FEM and less than 10% relative to the measurement.

Even beyond these specific models, this type of modeling framework allows the inclusion of complex effects, which cannot be analytically approximated within reasonable accuracy limits or numerically solved within reasonable time, within the main design optimization loop, thus ensuring the best quality solution of the global optimization.

REFERENCES

[1] C. W. T. McLyman, *Designing magnetic components for high frequency DC-DC converters*, en. KG Magnetics, Feb. 1993.

[2] C. P. Steinmetz, "On the law of hysteresis," *Proceedings of the IEEE*, vol. 72, no. 2, pp. 197–221, Feb. 1984.

[3] P. L. Dowell, "Effects of eddy currents in transformer windings," *Proc. of the Institution of Electrical Engineers*, vol. 113, no. 8, pp. 1387–1394, Aug. 1966.

[4] J. E. Huber and J. W. Kolar, "Solid-State Transformers: On the Origins and Evolution of Key Concepts," *IEEE Ind. Electron. Mag.*, vol. 10, no. 3, pp. 19–28, Sep. 2016.

[5] M. Mogorovic and D. Dujic, "100 kW, 10 kHz Medium-Frequency Transformer Design Optimization and Experimental Verification," *IEEE Transactions on Power Electronics*, vol. 34, no. 2, pp. 1696–1708, Feb. 2019.

[6] I. Villar, "Multiphysical Characterization of Medium-Frequency Power Electronic Transformers," PhD thesis, EPFL Lausanne, Switzerland, 2010.

[7] M. Bahmani, "Design and Optimization Considerations of Medium-Frequency Power Transformers in High-Power DC-DC Applications," PhD thesis, Chalmers University of Technology Gothenburg, Sweden, 2016.

[8] M. Mogorovic and D. Dujic, "Medium Frequency Transformer Leakage Inductance Modeling and Experimental Verification," in *IEEE Energy Conversion Congress and Exposition (ECCE) 2017*, Cincinnatti, OH, USA, 2017., pp. 419–424.

[9] S. Isler, T. Chaudhuri, D. Aguglia, and A. Bonnin, "Development of a 100 kW, 12.5 kV, 22 kHz and 30 kV Insulated Medium Frequency Transformer for Compact and Reliable Medium Voltage Power Conversion," in *Proceedings of the 19th European Conference on Power Electronics and Applications (EPE 2017 - ECCE Europe), Warsaw, Poland*, 2017.

[10] M. Luo, D. Dujic, and J. Allmeling, "Leakage Flux Modeling of Medium-Voltage Phase-Shift Transformers for System-Level Simulations," *IEEE Transactions on Power Electronics*, vol. 34, no. 3, pp. 2635–2654, Mar. 2019.

[11] P. Hammond, "Roth's method for the solution of boundary-value problems in electrical engineering," *Proceedings of the Institution of Electrical Engineers*, vol. 114, no. 12, pp. 1969–1976, Dec. 1967.

[12] A. Fouineau and et al., "Semi-Analytical Methods for Calculation of Leakage Inductance and Frequency-Dependent Resistance of Windings in Transformers," in *IEEE Transactions on magnetics, 2018.*, pp. 1–10.

[13] M. Luo, D. Dujic, and J. Allmeling, "Leakage Flux Modeling of Multiwinding Transformers for System-Level Simulations," *IEEE Transactions on Power Electronics*, vol. 33, no. 3, pp. 2471–2483, Mar. 2018.

[14] T. Gradinger, U. Drofenik, and S. Alvarez, "Novel Insulation Concept for an MV Dry-Cast Medium-Frequency Transformer," in *19th European Conference on Power Electronics and Applications (EPE'17 ECCE Europe)*, Warsaw, Poland, 2017., pp. 1–10.

[15] J. Smajic, T. Steinmetz, M. Rüegg, Z. Tanasic, R. Obrist, J. Tepper, B. Weber, and M. Carlen, "Simulation and measurement of lightning-impulse voltage distributions over transformer windings," *IEEE Transactions on Magnetics*, vol. 50, no. 2, pp. 553–556, Feb. 2014.

[16] T. Župan, B. Trkulja, R. Obrist, T. Franz, B. Cranganu-Cretu, and J. Smajic, "Transformer windings' rlc parameters calculation and lightning impulse voltage distribution simulation," *IEEE Transactions on Magnetics*, vol. 52, no. 3, pp. 1–4, Mar. 2016.

[17] G. Ortiz, "High-Power DC-DC Converter Technologies for Smart Grid and Traction Applications," PhD thesis, ETH Zurich, Switzerland, 2014.

[18] M. Mogorovic and D. Dujic, "Sensitivity Analysis of Medium Frequency Transformer Designs for Solid State Transformers," *IEEE Transactions on Power Electronics*, pp. 1–1, 2018.

Marko Mogorovic Marko Mogorovic (M'15) received the B.S. degree in electrical engineering from University of Belgrade, Belgrade, Serbia, in 2013 and M.S. degree in smart grid science and technology at École Polytechnique Fédérale de Lausanne (EPFL), Lausanne, Switzerland, in 2015. During his M.S., he spent one year at ABB Medium Voltage Drives, Turgi, Switzerland as a researcher. In 2019, he received his PhD degree from École Polytechnique Fédérale de Lausanne (EPFL) in Lausanne, Switzerland, where he is currently working as a postdoctoral researcher at the Power Electronics Laboratory. His current research interests include advanced modeling, design and optimization of galvanically isolated high power medium voltage converters.

Drazen Dujic Drazen Dujic (S'03-M'09-SM'12) received the Dipl.-Ing. and M.Sc. degrees from the University of Novi Sad, Novi Sad, Serbia, in 2002 and 2005, respectively, and the Ph.D. degree from the Liverpool John Moores University, Liverpool, U.K., in 2008, all in electrical engineering. From 2002 to 2006, he was with the Department of Electrical Engineering, University of Novi Sad as a Research Assistant, and from 2006 to 2009 with Liverpool John Moores University as a Research Associate. From 2009 till 2013, he was with ABB Corporate Research Centre, Switzerland, as a Principal Scientist working on the power electronics projects spanning the range from low-voltage/power SMPS in below kilowatt range to medium voltage high-power converters in a megawatt range. From 2013 till 2014, he was with ABB Medium Voltage Drives, Turgi, Switzerland, as R&D Platform Manager, responsible for ABB's largest IGCT based medium voltage drive - ACS6000. He is currently with Ecole Polytechnique Federale de Lausanne EPFL, Lausanne, Switzerland, as an Assistant Professor and the Director of the Power Electronics Laboratory. His current research interests include the areas of design and control of advanced high-power electronics systems and high performance drives. He has authored or coauthored more than 150 scientific publications and has filed 14 patents. He is an Associate Editor for IEEE Transactions on Industrial Electronics, IEEE Transaction on Power Electronics and IET Electric Power Applications. In 2018 he has received EPE Outstanding Service Award from European Power Electronics and Drives Association, and in 2014 the Isao Takahashi Power Electronics Award for outstanding achievement in power electronics.